DOI: 10.1093/jnci/djs188
Advance Access publication on April 18, 2012.

ARTICLE

Staging and Functional Characterization of Pheochromocytoma and Paraganglioma by ^{18}F-Fluorodeoxyglucose (^{18}F-FDG) Positron Emission Tomography

Henri J. L. M. Timmers, Clara C. Chen, Jorge A. Carrasquillo, Millie Whatley, Alexander Ling, Graeme Eisenhofer, Kathryn S. King, Jyotsna U. Rao, Robert A. Wesley, Karen T. Adams, Karel Pacak

Manuscript received June 20, 2011; revised March 7, 2012; accepted March 7, 2012.

Correspondence to: Karel Pacak, Program in Reproductive and Adult Endocrinology, Eunice Kennedy Shriver National Institutes of Child Health and Human Development, National Institutes of Health, Bldg 10, CRC 1E-3140, MSC 1109, 10 Center Dr, Bethesda 20892-1583, MD (e-mail: karel@mail.nih.gov).

Background Pheochromocytomas and paragangliomas (PPGLs) are rare tumors of the adrenal medulla and extra-adrenal sympathetic chromaffin tissues; their anatomical and functional imaging are critical to guiding treatment decisions. This study aimed to compare the sensitivity and specificity of ^{18}F-fluorodeoxyglucose positron emission tomography with computed tomography (^{18}F-FDG PET/CT) for tumor localization and staging of PPGLs with that of conventional imaging by [^{123}I]-metaiodobenzylguanidine single photon emission CT (^{123}I-MIBG SPECT), CT, and magnetic resonance imaging (MRI).

Methods A total of 216 patients (106 men, 110 women, aged 45.2 ± 14.9 years) with suspected PPGL underwent CT or MRI, ^{18}F-FDG PET/CT, and ^{123}I-MIBG SPECT/CT. Sensitivity and specificity were measured as endpoints and compared by the McNemar test, using two-sided *P* values only.

Results Sixty (28%) of patients had nonmetastatic PPGL, 95 (44%) had metastatic PPGL, and 61 (28%) were PPGL negative. For nonmetastatic tumors, the sensitivity of ^{18}F-FDG was similar to that of ^{123}I-MIBG but less than that of CT/MRI (sensitivity of ^{18}F-FDG = 76.8%; of ^{123}I-MIBG = 75.0%; of CT/MRI = 95.7%; ^{18}F-FDG vs ^{123}I-MIBG: difference = 1.8%, 95% confidence interval [CI] = −14.8% to 14.8%, $P = .210$; ^{18}F-FDG vs CT/MRI: difference = 18.9%, 95% CI = 9.4% to 28.3%, $P < .001$). The specificity was 90.2% for ^{18}F-FDG, 91.8% for ^{123}I-MIBG, and 90.2% for CT/MRI. ^{18}F-FDG uptake was higher in succinate dehydrogenase complex– and von Hippel–Lindau syndrome–related tumors than in multiple endocrine neoplasia type 2 (MEN2) related tumors. For metastases, sensitivity was greater for ^{18}F-FDG and CT/MRI than for ^{123}I-MIBG (sensitivity of ^{18}F-FDG = 82.5%; of ^{123}I-MIBG = 50.0%; of CT/MRI = 74.4%; ^{18}F-FDG vs ^{123}I-MIBG: difference = 32.5%, 95% CI = 22.3% to 42.5%, $P < .001$; CT/MRI vs ^{123}I-MIBG: difference = 24.4%, 95% CI = 11.3% to 31.6%, $P < .001$). For bone metastases, ^{18}F-FDG was more sensitive than CT/MRI (sensitivity of ^{18}F-FDG = 93.7%; of CT/MRI = 76.7%; difference = 17.0%, 95% CI = 4.9% to 28.5%, $P = .013$).

Conclusions Compared with ^{123}I-MIBG SPECT and CT/MRI, both considered gold standards for PPGL imaging, metastases were better detected by ^{18}F-FDG PET. ^{18}F-FDG PET provides a high specificity in patients with a biochemically established diagnosis of PPGL.

J Natl Cancer Inst 2012;104:700–708

Pheochromocytomas and paragangliomas (PPGLs) are rare catecholamine-producing tumors of the adrenal medulla and extra-adrenal sympathetic chromaffin tissues (1). Head and neck paragangliomas (HNPGLs) originate from vagal paraganglia. A large proportion of PPGLs and HNPGLs have a hereditary basis, often presenting as multiple tumors (2). These hereditary syndromes include multiple endocrine neoplasia type 2 (MEN2), von Hippel–Lindau (VHL) syndrome, neurofibromatosis type 1 (NF1), and paraganglioma syndromes associated with mutations of genes encoding subunits of the succinate dehydrogenase (SDH) complex, in particular subunits B (SDHB) and D (SDHD). *SDHB* mutations are associated with a particularly malignant phenotype (3,4).

In patients with a biochemically established diagnosis of PPGL (5), anatomical and functional imaging are critical to localize the primary tumor, evaluate its multiplicity, and detect metastases, all of which guide the physician's choice between curative surgery and palliative treatment. Computed tomography (CT) and magnetic resonance imaging (MRI) provide high sensitivity and allow precise delineation of the tumor. In most patients, anatomical imaging is complemented by functional imaging, which offers high specificity to positively identify the tumors as PPGL. The most widely used functional imaging technique is [^{123}I]-metaiodobenzylguanidine single photon emission computed tomography (^{123}I-MIBG SPECT). More recently, positron emission tomography (PET) has been

used with radiopharmaceuticals such as 6-[^{18}F]-fluorodopamine (^{18}F-FDA) and [^{18}F]-fluoro-dihydroxyphenylalanine (^{18}F-FDOPA), which specifically target the catecholamine biosynthetic and storage pathways of PPGL tumor cells (6–8).

Among PET tracers, 2-[^{18}F]-fluoro-2-deoxy-D-glucose (^{18}F-FDG) has not previously been considered to be a first-line functional imaging agent for PPGL, even though it has been used this way for other tumors (9), possibly because there is a concern that it may accumulate nonspecifically and provide low sensitivity for benign PPGL. The degree of ^{18}F-FDG uptake mirrors glucose uptake and metabolism in various tumors (10). In malignant PPGL and especially in *SDHB*-related PPGL, metastases are more accurately detected by ^{18}F-fluorodeoxyglucose positron emission tomography with computed tomography (^{18}F-FDG PET/CT) than by ^{123}I-MIBG SPECT (8,11,12). Prominent ^{18}F-FDG uptake by *SDHB*-related metastases has been suggested to be a hallmark of altered glucose metabolism related to genotype-specific tumor cell biology (13). ^{18}F-FDG PET/CT has also been successfully applied in the localization of primary nonmetastatic PPGL, yielding a sensitivity similar to ^{123}I-MIBG (8). Therefore, ^{18}F-FDG has the potential to be useful in PPGL imaging, not only for detection of metastases but also as a tool for functional characterization that identifies tumors with a high metabolic rate and high metastatic potential.

The aims of the this study were 1) to establish the sensitivity and specificity of ^{18}F-FDG PET for the localization of various genetically-derived nonmetastatic and metastatic PPGLs, 2) to provide a strategy for optimal staging of PPGL and HNPGL by comparing ^{18}F-FDG PET with the standard imaging techniques (CT, MRI, ^{123}I-MIBG SPECT), and 3) to investigate whether functional imaging using ^{18}F-FDG PET might provide clues for a genetic diagnosis underlying PPGL.

CONTEXT AND CAVEATS

Prior knowledge

Conventionally, [^{123}I]-metaiodobenzylguanidine single photon emission computed tomography (^{123}I-MIBG SPECT), computed tomography (CT), and magnetic resonance imaging (MRI) are used to image pheochromocytomas and paragangliomas (PPGLs). These authors compared ^{18}F-fluorodeoxyglucose positron emission tomography with computed tomography (^{18}F-FDG PET/CT) with conventional imaging for tumor localization and staging.

Study design

A total of 216 patients with suspected PPGL were tested by each of the four imaging techniques. Sensitivity and specificity of the techniques were then compared.

Contribution

For nonmetastatic tumors, ^{18}F-FDG PET/CT was similar to ^{123}I-MIBG but less than CT/MRI in sensitivity; it was similar to CT/MRI and slightly less than ^{123}I-MIBG in specificity. For metastases, ^{18}F-FDG and CT/MRI were more sensitive than ^{123}I-MIBG, and for bone metastases, ^{18}F-FDG was more sensitive than CT/MRI.

Implication

^{18}F-FDG PET/CT is better than ^{123}I-MIBG and CT/MRI, the current standard techniques, at detecting PPGL metastases.

Limitations

The sample size of patients with hereditary nonmetastatic PPGLs and HNPGL was relatively small. Further studies are warranted to assess the full impact of genotypes on functional imaging results.

From the Editors

Methods

Patients

Between 2003 and 2010, we prospectively studied 216 consecutive patients (106 men and 110 women, aged [mean ± SD] 45.2 ± 14.9 years), who underwent ^{18}F-FDG scanning as part of their evaluation for suspected PPGL. All patients were investigated at a single center, the National Institutes of Health. The final diagnosis was based on biochemical findings, imaging results, and clinical follow-up. Among the 216 patients, there were 60 (28%) patients with one or multiple foci of nonmetastatic PPGL, 95 (44%) patients with metastatic PPGL, and 61 (28%) patients without evidence of PPGL after detailed evaluation. Metastatic PPGL was defined by the presence of metastatic lesions at sites where chromaffin tissue is normally absent.

PPGL-negative patients had been referred for one or more of the following reasons: 1) symptoms and signs highly suggestive of PPGL; 2) adrenal incidentaloma; 3) a predisposing hereditary disorder associated with the presence of PPGL, including proven mutation carriers and patients with a positive family history and typical signs and symptoms of catecholamine excess; or 4) evaluation for recurrent disease. PPGL was ruled out by normal plasma metanephrine levels, imaging studies, and close clinical follow-up. Patient characteristics are listed in Table 1 and Supplementary Tables 1–3 (available online).

There were 66 patients with germline *SDHB* mutations, 12 with *SDHD* mutations, and 10 with *RET*-related MEN2, four patients with VHL syndrome, and one with *NF1* mutation. Genetic testing included gene sequencing of *SDHB*, *SDHD*, *RET*, and *VHL* and assessment of large gene rearrangements of *SDHB* and *SDHD*. Patients were not tested for mutations in the recently described genes *SDHA* (14), *SDHAF2* (15), and *TNEM127* (16). Imaging results of 51 patients were also included in a previous report that focused on ^{18}F-FDOPA PET (8). The protocol (00-CH-0093) was approved by the Institutional Review Board of the Eunice Kennedy Shriver National Institutes of Child Health and Development, National Institutes of Health. All patients provided written informed consent.

Functional Imaging

All functional imaging studies were performed at a single center, the Department of Nuclear Medicine of the National Institutes of Health in Bethesda, MD. Cameras and radiopharmacy equipment were subject to frequent quality control according to institutional standards and protocols. ^{18}F-FDG PET(/CT) and ^{123}I-MIBG SPECT(/CT) were performed as described previously (11,17). The initial six patients underwent ^{18}F-FDG PET just before the implementation of PET/CT in our protocol early in 2003. Since then, all PET/CT studies have been performed on the same instrument (GE Discovery ST, GE Healthcare, Chalfont St. Gilles, United Kingdom), using the same protocol (11,17). With regard to ^{123}I-MIBG scanning,

Table 1. Characteristics and imaging results in patients with hereditary primary (nonmetastatic) pheochromocytoma and paraganglioma (PPGL)*

Sex	Age, y	Germline mutation	NMN (upper reference limit = 112 pg/mL)	MN (upper reference limit = 61 pg/mL)	Prior PPGL surgery	Tumor location	Tumor size (dimensions or maximum diameter, cm)	FDG	SUV	CT/MRI	MIBG
F	52	SDHB	846	19	—	Extra-adrenal abdominal	7.5	+	12.4	+	+
M	53	SDHB	66	<48	—	Extra-adrenal abdominal	2 × 1.3	+	8.7	+	−
M	31	SDHB	35	33	—	Extra-adrenal abdominal	7 × 7.5 × 4.3	+	14.1	+	+
F	36	SDHB	370	35	—	Mediastinal	2.7 × 1.6	+	19.5	+	−
F	30	SDHB	1325	9	—	L adrenal	7.5 × 5.4 × 3.8	+	4.7	+	+
M	31	SDHD	1758	23	HNPGL resection	Myocardial	3.3 × 2.5 × 1.8	+	10.9	+	−
						L adrenal	7.5 × 5.2 × 3.6	+	16.4	+	+
						R adrenal	10.5 × 3.2 × 3.4	+	14.9	+	+
M	52	SDHD	291	21	Biopsy	Mediastinal	6	+	13.7	+	+
M	61	SDHD	137	33	—	R adrenal	2.3 × 2 × 1.8 + 2.1 × 1.6 × 1.4	+	11.9	+	+
M	23	VHL	3645	30	—	L adrenal	3.2 × 2.8 × 1.8	+	7.7	+	+
						R adrenal	6.7 × 6.0 × 3.5	+	11.7	+	+
M	32	VHL	1159	23	—	L adrenal	2.7 × 2.2 × 2	+	30.7	+	+
						R adrenal	2.7 × 2.7 × 1.5	+	19.8	+	+
F	41	MEN2	125	217	L + R adrenalectomy	L adrenal	1.5	−	2.5	−	+
F	32	MEN2	746 (<419)	1300 (<180)	—	L adrenal	2.5 × 2 × 2 + 2.8 × 1.5 × 1.4 + 1.3 × 1.1 × 0.6	−	2.1	+	+
			(Urine)	(Urine)		R adrenal	2.1	−	1.9	+	+
F	40	MEN2	289	105	L + R adrenalectomy	R adrenal	3.5 × 3.2 × 2	−	1.9	+	+
F	39	MEN2	2563	2350	—	L adrenal	1	−	1.8	+	+
		MEN2	2563	2350	—	R adrenal	12 × 8 × 6.5	+	3.3	+	+
F	45	MEN2	105	84	L + R adrenalectomy	L adrenal	1 × 1 × 0.6 + 2	+	4.2	+	
F	26	MEN2	180	68	—	L adrenal	1 × 0.8 × 1.5 + 1.5 × 1.2 × 2	−	1.9	+	+
M	57	MEN2	135	144	R adrenalectomy	L adrenal	1.5 × 1.3 × 1	+	3.2	+	+
F	38	MEN2	84	586	L + R adrenalectomy	L adrenal	3 × 2	+	6.4	+	+
M	27	NF1	397	1685	—	R adrenal	8.5 × 6 × 5	+	5.2	+	+

* CT = computed tomography; F = female; FDG = ^{18}F-fluorodeoxyglucose positron emission tomography; HNPGL = head and neck PGL; L = left; M = male; MEN2 = multiple endocrine neoplasia type 2; MIBG = [^{123}I]-metaiodobenzylguanidine single photon emission computed tomography; MN = plasma metaneprine; MRI = magnetic resonance imaging; NF1 = neurofibromatosis type 1; NMN = plasma normetanephrine; PPGL = pheochromocytoma or paraganglioma; R = right; SDHB/C/D/x = succinate dehydrogenase subunit B/C/D/x; SUV = standard uptake value; VHL = Von Hippel-Lindau syndrome.

SPECT/CT instead of SPECT alone was performed in 40 (23.1%) of 173 MIBG scans when the technology became available in 2009. Camera-wise whole-body planar and SPECT-only images were done on a variety of cameras—either a three-headed (Tronix, Meditronix, New Delhi, India) camera or one of our various two-headed gamma cameras (either Siemens, Munich, Germany or Phillips/Adac, Milpitas, CA). ^{123}I-MIBG scans were performed within 2 weeks of the ^{18}F-FDG scans in random order, with the exception of five ^{123}I-MIBG scans that were performed within 2–6 weeks. ^{123}I-MIBG scans were performed in 55 patients (92%) with nonmetastatic PPGL, in 77 patients (81%) with metastatic PPGL, and in 41 patients (67%) without PPGL.

CT and MRI

All anatomical imaging studies were performed at a single center, the Department of Radiology of the National Institutes of Health in Bethesda, MD. CT scans were performed using LightSpeed Ultra, LightSpeed QX/i (General Electric Healthcare Technologies, Waukesha, WI) and Mx8000 IDT (Philips Medical Systems, Andover, MA) scanners. Section thickness was 2–2.5 mm in the neck and 5 mm through the chest, abdomen, and pelvis. Studies were performed with a rapid infusion of nonionic water soluble contrast agent, as well as oral contrast material.

MRI scans were obtained using 1.5 or 3 T scanners (General Electric Healthcare Technologies and Philips Medical Systems). Image thickness was 5 mm for neck studies and 5–8 mm for other body regions. Studies included injection of a gadolinium-DTPA contrast agent, using fat-suppressed T1-weighted gradient-echo imaging, generally in both axial and coronal planes.

The following body regions were imaged by CT and/or MRI: neck, chest, abdomen, and pelvis in 189 patients; chest, abdomen, and pelvis in 12 patients; neck, abdomen, and pelvis in two patients; neck and abdomen in three patients; neck and pelvis in one patient; abdomen only in three patients; and neck only in two patients.

Analysis of Data

CT and MRI scans were read by radiologists as part of the clinical routine. Lesions that were "typical" or "highly suspicious" for PPGL were considered positive. ^{18}F-FDG and ^{123}I-MIBG scans were read by two nuclear medicine physicians (C. C. Chen and J. A. Carrasquillo) who were blinded to the results of all other imaging studies. Whenever there were discrepancies between the two reports, a consensus reading was performed. Focal areas of abnormal uptake not corresponding to normal physiological sites of accumulation for each of the tracers were considered as lesions. Lesions were graded on a scale of 1–5 (1 = not PPGL, 2 = doubtful, 3 = equivocal, 4 = probable, 5 = definite PPGL). Only lesions with scores of 4 and 5 were counted as positive findings.

HNPGLs were analyzed separately from sympathetic PPGL because they appear to have very different functional imaging properties (18). Data from patients with HNPGLs were included only if data from an MRI specifically targeted at HNPGL were available as a standard. Without MRI imaging, head and neck lesions seen by ^{18}F-FDG PET/CT were not scored.

For calculations of sensitivity, two different standards were used. For patients with primary nonmetastatic PPGL, histopathologically confirmed PPGLs served as reference. For metastatic PPGL, sensitivity was calculated in reference to lesions detected by any imaging in the following locations: 1) retroperitoneum or mediastinum, 2) bone, 3) liver, and 4) lungs. Thus, each region was scored as tumor positive or negative (region-based sensitivity).

For ^{18}F-FDG scans, uptake in normal adrenals and primary PPGLs was also assessed. Maximum standardized uptake values (SUVs) corrected for the lean body mass were calculated (SUV = [No. of Ci/g] × [lean body mass in g/No. of Ci injected]). Patients with PPGL-negative adrenal glands with an abnormal appearance on CT or MRI (eg, other adrenal tumors) were excluded from the analysis. Maximum SUVs were determined in manually drawn regions of interest over adrenal PPGLs and normal adrenal glands, as delineated by CT. SUV was not calculated for right adrenal glands if there was difficulty separating it from physiological uptake in the liver. Liver-normalized SUVs were calculated as PPGL and adrenal gland maximum SUVs divided by corresponding liver mean SUVs. Regions of interest were drawn in four consecutive slices in the upper central liver to obtain mean liver SUVs.

Statistical Analysis

Results are given as means with 95% confidence intervals (CIs) unless stated otherwise. The McNemar test was used to compare sensitivities and specificities between different imaging modalities. To compare sensitivities of a particular imaging modality between subgroups of patients, that is, comparison of independent observations, a Fisher exact test was used. For the comparison of different imaging modalities within subgroups (paired observations), we used the McNemar test. For comparison of SUVs of hereditary non–epinephrine-producing tumors and other tumors, analysis of variance and post hoc analysis using the Tukey–Kramer test were performed (19). A two-sided P less than .05 was considered to be statistically significant. Statistical analysis was performed using the Statistical Package for the Social Sciences (SPSS for Windows 12; SPSS Inc, Chicago, IL) and the JMP statistics software package (SAS Institute, Cary, NC); the latter was used for analysis of variance with post hoc testing by the Tukey–Kramer test.

Results

Nonmetastatic PPGL

Among 60 patients, 69 nonmetastatic PPGLs were histopathologically identified, of which 53 were adrenal and 16 extra-adrenal in location (Table 1 and Supplementary Table 1, available online). CT and/or MRI as well as ^{18}F-FDG PET were performed for all patients. ^{123}I-MIBG scintigraphy was performed in all except five patients. Three MEN2 patients with benign adrenal PPGLs (F38, F32, and F48; Table 1) had metastatic medullary thyroid cancer, and one patient with a sporadic benign adrenal PPGL also had a metastatic esophageal anaplastic adenocarcinoma (Supplementary Table 1, available online). For these patients, only the adrenal lesions were included in the analysis.

Sensitivity of ^{18}F-FDG was similar to ^{123}I-MIBG but less than CT/MRI (sensitivity of ^{18}F-FDG = 76.8%; of ^{123}I-MIBG = 75.0%; of CT/MRI = 95.7%; ^{18}F-FDG vs ^{123}I-MIBG: difference = 1.8%, 95% CI = −14.8% to 14.8%, P = .210; ^{18}F-FDG vs CT/MRI: difference = 18.9%, 95% CI = 9.4% to 28.3%, P < .001, two-sided McNemar test). Two false-positive findings were seen. ^{123}I-MIBG showed a false-positive left adrenal focus in addition to the true-positive right adrenal PPGL (M18, sporadic, Supplementary Table 1, available online). CT showed a false-positive sub-centimeter left adrenal nodule in addition to a true right adrenal PPGL (M61, SDHD; Table 1). Clinical and biochemical follow-up at 1 and 4 years after unilateral PPGL resection, respectively, showed no evidence of disease in these two patients. In one patient, ^{18}F-FDG showed a lung lesion (sporadic, F54; Table 1), which was subsequently found to be non–small cell lung cancer. The lesion was also visible on CT/MRI. Six ^{18}F-FDG scans demonstrated uptake in brown fat.

The sensitivity of ^{18}F-FDG was 100% in SDHB/D and VHL mutation carriers compared with 40% in MEN2. The sensitivity of ^{123}I-MIBG was 80% in SDHB/D and VHL compared with 100% in MEN2. Representative examples are shown in Figure 1. There were no statistically significant differences in sensitivity of functional imaging for detecting adrenal vs extra-adrenal PPGL, regardless of genetic background (^{18}F-FDG: 73.6% vs 68.8% and ^{123}I-MIBG: 79.6% vs 60%). Also, functional imaging results were independent of biochemical phenotype that is, epinephrine ± norepinephrine-producing vs norepinephrine-only producing (data not shown).

Metastatic PPGL

All 95 patients with metastatic PPGL underwent ^{18}F-FDG PET. ^{123}I-MIBG scintigraphy was done in 79 patients (83%). CT and/or MRI within 3 months from ^{18}F-FDG-PET was available for all but one patient. Individual findings are shown in Supplementary Table 2 (available online).

Region-based sensitivity, as indicated in Table 2, was greater for ^{18}F-FDG and CT/MRI than for ^{123}I-MIBG (sensitivity of ^{18}F-FDG = 82.5%; of ^{123}I-MIBG = 50.0%; of CT/MRI = 74.4%;

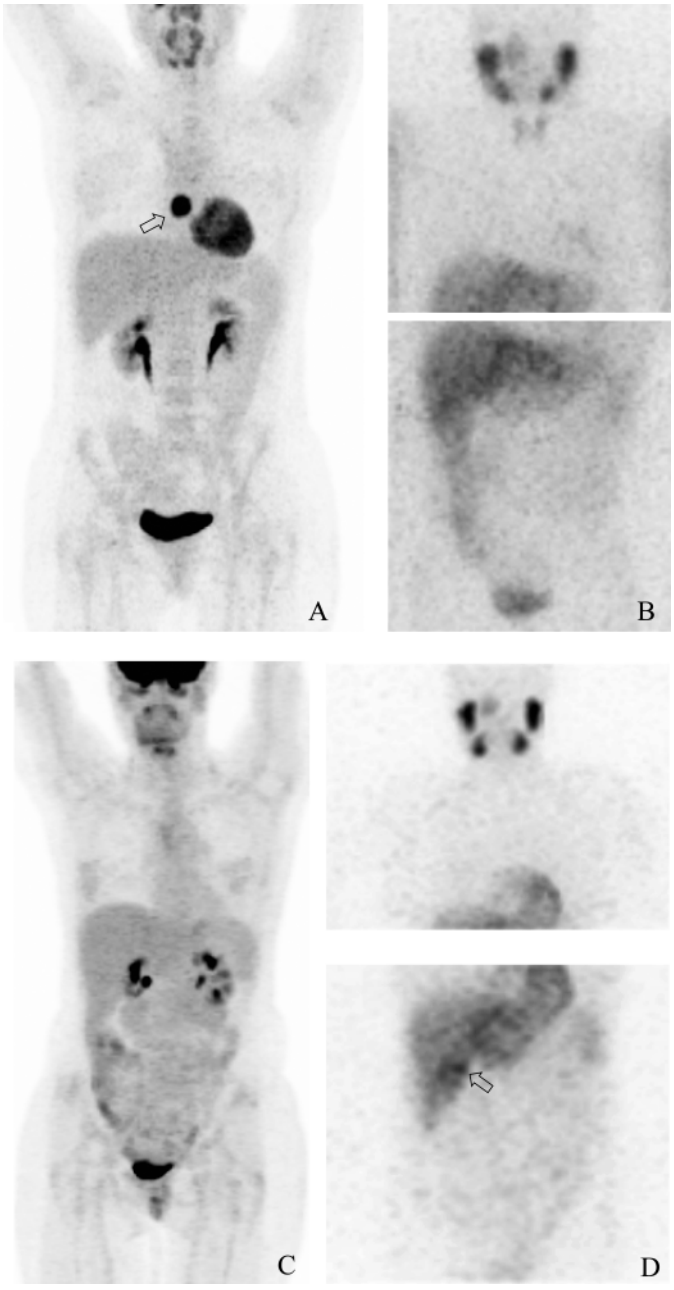

Figure 1. ^{18}F-fluorodeoxyglucose positron emission tomography (^{18}F-FDG) and [^{123}I]-metaiodobenzylguanidine (^{123}I-MIBG) images of patients with succinate dehydrogenase subunit B (*SDHB*) mutations and multiple endocrine neoplasia-2 (MEN2). **A** and **B**) Maximum intensity projected ^{18}F-fluorodeoxyglucose positron emission tomography (^{18}F-FDG PET) (**A**) and [^{123}I]-metaiodobenzylguanidine (^{123}I-MIBG) scintigraphy (SPECT) (**B**) of an SDHB patient with a paraganglioma of the mediastinum (Table 1: *SDHB*, F36): lesion marked by **arrow**. **C** and **D**) Maximum intensity projected ^{18}F-FDG PET (**C**) and ^{123}I-MIBG scintigraphy (**D**) of an MEN2 patient with a right adrenal pheochromocytoma (Table 1: *MEN2*, F40): lesion marked by **arrow**.

^{18}F-FDG vs ^{123}I-MIBG: difference = 32.5%, 95% CI = 22.3% to 42.5%, $P < .001$; CT/MRI vs ^{123}I-MIBG: difference = 24.4%, 95% CI = 11.3% to 31.6%, $P < .001$; two-sided McNemar test). In 26 patients (33%), ^{123}I-MIBG was false negative. ^{18}F-FDG was false negative in five patients (5.3%) and CT/MRI in 11 (11.7%).

Sensitivities were compared between 52 *SDH* patients (47 of whom had *SDHB* mutations and five of whom had *SDHD* mutations) and 23 non-*SDH* patients (including one with a *VHL* mutation and one with MEN2). Sensitivity of ^{18}F-FDG was greater in *SDH* patients than in non-*SDH* patients (sensitivity in *SDH* patients = 92.0%; in non-*SDH* patients = 67.3%; difference = 24.7%, $P < .001$; two-sided Fisher exact test) (Table 3), whereas ^{123}I-MIBG scintigraphy performed worse in *SDH* tumors than in non-*SDH* tumors (sensitivity in *SDH* patients = 44.6%; in non-*SDH* patients = 65.9%; difference = 21.3%, $P = .027$; two-sided Fisher exact test). There were no false-negative ^{18}F-FDG scans among *SDH* patients.

Specifically for bone metastases, ^{18}F-FDG was more sensitive than CT/MRI (sensitivity of ^{18}F-FDG = 93.7%; of CT/MRI = 76.7%; difference = 17.0%, 95% CI = 4.9% to 28.5%, $P = .0129$; two-sided McNemar test) (Table 4).

PPGL Ruled Out

In the 61 patients in whom PPGL was ruled out, several false-positive lesions were found by imaging (Supplementary Table 3, available online). After exclusion of low enhancing adrenal nodules with an "adenoma-like" appearance according to the radiologists, the specificity of CT/MRI was 90.2% (six false-positive scans). If all adrenal nodules on CT/MRI were included, the specificity decreased to 70.5% (18 false-positive scans). The specificity of ^{18}F-FDG PET was 90.2% (six false-positive scans) and for ^{123}I-MIBG, it was 91.8% (five false-positive scans). Among the six "false-positive" lesions on ^{18}F-FDG PET, three were subsequently identified as left renal cell carcinoma (SDHB, M62; Supplementary Table 5, available online), gastrointestinal stromal tumor (SDHB, M72), and left breast ductal carcinoma (sporadic, F57). The first two lesions were also visible on CT/MRI but were not considered as PPGL by the radiologists. On ^{18}F-FDG, brown fat was seen in three patients. The false-positives seen with ^{123}I-MIBG scintigraphy were all due to visualization of presumably normal adrenal glands.

Head and Neck Paraganglioma

A total of 26 HNPGLs were found on CT/MRI in 19 patients (Supplementary Table 6, available online). ^{18}F-FDG was more sensitive than ^{123}I-MIBG (sensitivity of ^{18}F-FDG = 85% [22/26]; of ^{123}I-MIBG = 52% [11/21]; difference = 33%, 95% CI = 8.6% to 53.0%, $P = .021$; two-sided McNemar test).

^{18}F-Fluorodeoxyglucose Positron Emission Tomography With Computed Tomography Standardized Uptake Values

SUVs were statistically significantly higher ($P < .001$) for adrenal PPGL (5.0 ± 5.5) and extra-adrenal PPGL (8.5 ± 5.5) than for normal adrenal glands (1.6 ± 0.8) (Figure 2). There was, however, considerable overlap between the groups. Liver-normalized SUVs showed similar differences: adrenal PPGL, 2.84 ± 3.70 (range = 0.47–17.3); extra-adrenal PPGL, 5.21 ± 3.23; normal adrenal glands of patients without PPGL, 0.84 ± 0.26.

A receiver operating curve was constructed from maximum SUVs of adrenal PPGLs and normal adrenals in patients with nonmetastatic PPGL. The area under curve was 0.921 (Figure 3). To provide 100% sensitivity, the upper reference for a normal SUV was established at 1.1 (the minimum value for adrenal PPGL), resulting in a specificity of 73%. To provide 100% specificity, the upper reference for normal was established at 4.6 (the

Table 2. Sensitivity of imaging*

Imaging method	Nonmetastatic primary PPGL		Metastases		Primary head and neck PGL	
	No. positive/No. of tumors	% (95% CI)	No. positive /No. of tumor regions	% (95% CI)	No. positive/No. of tumors	% (95% CI)
^{18}F-FDG PET†	53/69	76.8 (66.6 to 87.0)	170/206	82.5 (77.3 to 87.8)	18/26	69.2 (50.2 to 88.2)
^{123}I-MIBG SPECT‡	48/64	75.0 (64.1 to 85.9)	86/172	50.0 (42.5 to 57.6)	7/21	33.3 (11.4 to 55.3)
CT/MRI	66/69	95.7 (90.7 to 100.6)	148/199	74.4 (68.3 to 80.5)	N/A	N/A

* Sensitivities are expressed as the number of positive body regions/the total number of tumor-positive regions, with percentages and 95% CIs. CI = confidence interval; CT/MRI = computed tomography with magnetic resonance imaging; ^{18}F-FDG PET = [^{18}F]-fluorodeoxyglucose positron emission fluorography; ^{123}I-MIBG SPECT = [^{123}I]-metaiodobenzylguanidine single photon emission computed tomography; N/A = not applicable; PPGL = pheochromocytoma and paraganglioma.

† For nonmetastatic primary PPGL; ^{18}F-FDG vs ^{123}I-MIBG ns, FDG vs CT/MRI $P < .001$; within metastases; ^{18}F-FDG vs ^{123}I-MIBG $P < .001$, FDG vs CT/MRI $P = .08$; within primary head and neck PGL; ^{18}F-FDG vs ^{123}I-MIBG $P = .031$ (McNemar test, two-sided).

‡ For nonmetastatic primary PPGL; ^{123}I-MIBG vs CT/MRI $P = .002$; within metastases; ^{123}I-MIBG vs CT/MRI $P < .001$ (McNemar test, two-sided).

maximum value for PPGL-negative normal adrenals), resulting in a sensitivity of 82%.

The distribution of SUVs in nonmetastatic PPGLs across hereditary and sporadic tumors is shown in Figure 4. The maximum SUVs for hereditary non–epinephrine-producing tumors (SDHB, SDHD, VHL) was statistically significantly higher (14.3 ± 6.3, $P < .05$) than for hereditary epinephrine-producing tumors (MEN2, NF1: 3.1 ± 1.5), sporadic non–epinephrine-producing tumors (7.0 ± 6.0) and sporadic epinephrine-producing tumors (3.8 ± 1.6).

Linear regression analysis revealed a statistically significant ($P < .001$) relationship between metanephrine levels and SUV with a correlation coefficient of 0.58.

Discussion

^{18}F-FDG PET/CT scanning is an established technique for tumor staging and follow-up (9). The findings of the this large prospective study indicate that the usefulness of ^{18}F-FDG for tumor imaging certainly also pertains to PPGLs. Primary PPGLs are equally well identified by ^{18}F-FDG PET/CT and ^{123}I-MIBG SPECT(/CT), currently the standard modality. Metastases are better detected by ^{18}F-FDG PET than by ^{123}I-MIBG SPECT, with sensitivities of 80% and 49%, respectively. In fact, one-third of patients with metastatic PPGL had false-negative ^{123}I-MIBG scans. Moreover, for the localization of metastases of the bone, a frequent site of involvement in malignant PPGL, ^{18}F-FDG PET, was superior to whole-body CT and/or MRI (sensitivity 94% vs 79%), whereas for soft tissue metastases, the performance was similar.

Regarding the specificity of ^{18}F-FDG PET, tracer uptake by non-PPGL lesions and by normal adrenal glands might be of concern. This study shows, however, that a very limited number of otherwise unexplained extra-adrenal ^{18}F-FDG foci were encountered. In most patients, ^{18}F-FDG uptake by normal adrenal glands did not exceed that of the liver (20). The distinction between pathological and physiological ^{18}F-FDG accumulation is facilitated by the calculation of SUV. The diagnosis of adrenal PPGL is highly unlikely when the ^{18}F-FDG SUV is below 1.1 and very likely when it exceeds 4.6. These cutoffs correspond with 100% sensitivity and specificity, respectively.

Hereditary syndromes are associated with PPGL features such as catecholamine profile, tumor location, and malignant potential (21). Our current findings and previous observations (11,22) provide evidence that genotypes also determine the results of functional imaging. For nonmetastatic PPGL, we found that *SDH*- and *VHL*-related tumors are without exception detected by ^{18}F-FDG PET, whereas the majority of MEN2-related PPGLs are ^{18}F-FDG PET negative. SUVs were higher for *SDH*- and *VHL*-related tumors than for MEN2- and NF1-related tumors. For metastatic PPGL, we confirm that the sensitivity of ^{18}F-FDG PET is higher in *SDHB/D*-related than non–*SDHB/D*-related lesions (8,11). Apparently, genotype-specific tumor cell biology translates into distinct patterns of radiotracer uptake and accumulation.

The *SDH* genes encode the mitochondrial enzyme SDH, which is complex II of the mitochondrial respiratory chain and catalyzes the oxidation of succinate to fumarate in the Krebs cycle. *SDH* mutations lead to loss of SDH enzymatic activity and induction of hypoxic- and angiogenic-responsive genes (23). A similar

Table 3. Region-based sensitivity of imaging in metastases with and without succinate dehydrogenase subunit B and D (*SDHB* and *SDHD*) mutations*

Imaging method	*SDHB, SDHD*		non-*SDHx*		*P*
	No. positive/No. of tumor regions	% (95% CI)	No. positive/ No. of tumor regions	% (95% CI)	
^{18}F-FDG PET	103/112	92.0 (86.9 to 97.1)	37/55	67.3 (54.5 to 80.1)	<.001
^{123}I-MIBG SPECT	41/92	44.6 (34.2 to 54.9)	29/44	65.9 (51.3 to 80.5)	.027
CT/MRI	84/107	78.5 (70.6 to 86.4)	39/55	70.9 (58.5 to 83.3)	.333

* Sensitivities are expressed as the number of positive body regions/the total number of tumor-positive regions, with percentages and 95% CIs. CI = confidence interval; CT/MRI = computed tomography with magnetic resonance imaging; ^{18}F-FDG PET = [^{18}F]-fluorodeoxyglucose positron emission fluorography; ^{123}I-MIBG SPECT = [^{123}I]-metaiodobenzylguanidine single photon emission computed tomography; PGL = paraganglioma; PPGL = pheochromocytoma and paraganglioma. Among patients with SDH mutations: ^{18}F-FDG vs ^{123}I-MIBG, $P < .001$; ^{18}F-FDG vs CT/MRI, $P = .009$; ^{123}I-MIBG vs CT/MRI, $P < .001$ (Fisher exact test, two-sided).

Table 4. Sensitivity of imaging in metastases to soft tissue regions vs bone regions*

Imaging test	Soft tissue		Bone		
	No. positive/No. of tumor regions	% (95% CI)	No. positive/No. of tumor regions	% (95% CI)	*P*
^{18}F-FDG PET	111/143	77.6 (70.7 to 84.5)	59/63	93.7 (87.5 to 99.8)	.005†
^{123}I-MIBG SPECT	54/119	45.4 (36.3 to 54.5)	32/52	61.5 (47.9 to 75.2)	.067†
CT/MRI	102/139	73.4 (65.9 to 80.8)	46/60	76.7 (65.7 to 87.7)	.724†

* Sensitivities are expressed as the number of positive body regions/the total number of tumor-positive regions, with percentages and 95% CIs. CI = confidence interval; CT/MRI = computed tomography with magnetic resonance imaging; ^{18}F-FDG PET = [^{18}F]-fluorodeoxyglucose positron emission fluorography; ^{123}I-MIBG SPECT = [^{123}I]-metaiodobenzylguanidine single photon emission computed tomography; PGL = paraganglioma; PPGL = pheochromocytoma and paraganglioma.

† Fisher exact test, two-sided. Within soft tissue: ^{18}F-FDG vs ^{123}I-MIBG $P < .001$; ^{123}I-MIBG vs CT/MRI, $P < .001$ (McNemar test, two-sided). Within bone: ^{18}F-FDG vs ^{123}I-MIBG P < .001; ^{18}F-FDG vs CT/MRI, $P = .0129$ (McNemar test, two-sided).

pattern is observed in *VHL*-related PPGL (24). These mechanisms may cause tumor cells to shift to aerobic glycolysis, a phenomenon known as the Warburg effect (25). We suggest that this in turn leads to increased expression of glucose transporters and ^{18}F-FDG uptake, explaining the success of ^{18}F-FDG PET in *SDH*- and *VHL*-related PPGL. This awaits confirmation on a molecular level. *RET*- and *NF1*-related tumorigenesis is attributed to the deregulation of the RAS/RAF/MAP kinase signaling cascade (26), a pathway that is not expected to directly impact glucose metabolism and ^{18}F-FDG uptake. When comparing ^{18}F-FDG uptake by nonmetastatic PPGLs across different genotypes, SUVs were generally higher in *SDHB/D* and *VHL* than in MEN2 and NF1 tumors. Among tumors of the same genotype, however, SUVs varied considerably and overlapped with SUVs of sporadic tumors, precluding dependable genotyping in individual patients based on SUV. For ^{123}I-MIBG no genotype-specific differences could be distinguished.

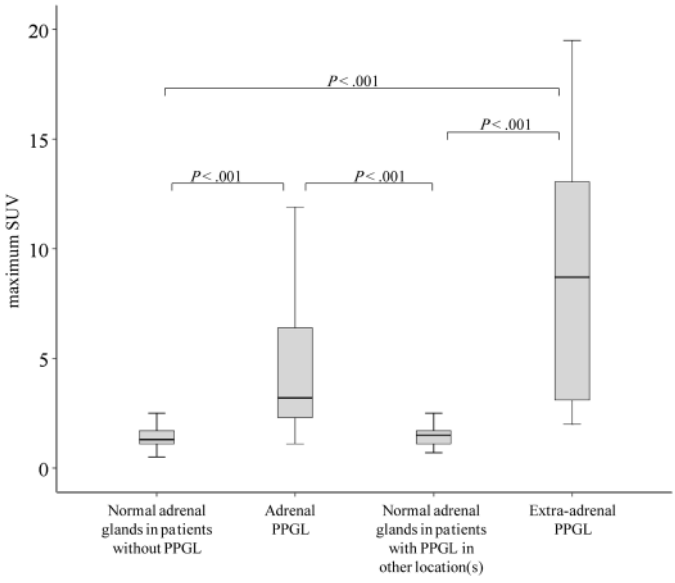

Figure 2. ^{18}F-fluorodeoxyglucose positron emission tomography standardized uptake value (SUV) in pheochromocytoma and paraganglioma (PPGL) vs normal adrenal glands. Box and whiskers diagrams of maximum SUVs are statistically significantly higher for adrenal and extra-adrenal PPGLs than for normal adrenal glands in patients without PPGL and contralateral adrenal or extra-adrenal PPGL (**boxes** indicate 25th and 75th percentile, **solid lines** indicate median, and **whiskers** indicate range) (Tukey–Kramer test, two-sided).

Besides the diagnostic qualities of ^{18}F-FDG PET (27,28), advantages over ^{123}I-MIBG SPECT are higher resolution and a shorter interval between tracer injection (1 hour vs 24–48 hours). Among PET tracers, ^{18}F-FDG is most widely available. Other useful tracers, such as [^{18}F]-fluorodopamine (7,29) and ^{18}F-FDOPA (8,30), are less accessible.

The results obtained from this large prospective study translate into important considerations for the use and interpretation of ^{18}F-FDG PET in PPGL in clinical practice. Before any imaging, a biochemical diagnosis of PPGL should be established by blood and/or urine examinations. For subsequent tumor localization, we show that ^{18}F-FDG PET has clear advantages over ^{123}I-MIBG scanning as the first-line functional imaging modality. Furthermore, ^{18}F-FDG PET can be used along with syndromal features, family history, age, tumor location, and catecholamine phenotype (31) to guide the genetic testing strategy in individual patients, prioritizing *SDH* and *VHL* testing in those with prominent ^{18}F-FDG uptake (SUV > 5). For the follow-up of patients with established metastatic PPGL, ^{18}F-FDG is more sensitive than ^{123}I-MIBG, especially in patients with *SDH*-related tumors, and should be performed in addition to CT or MRI to establish the full extent of

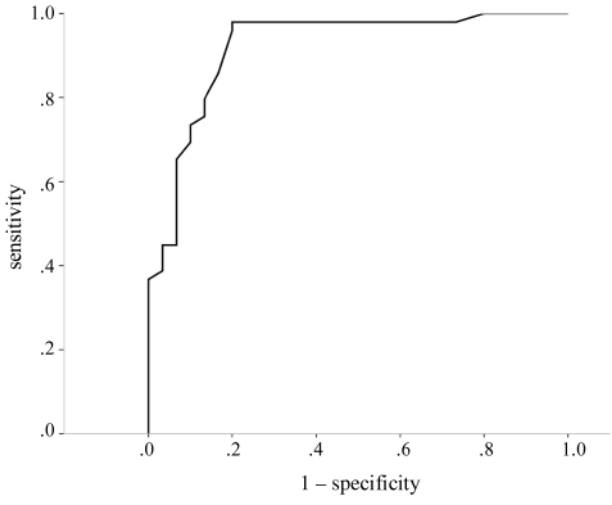

Figure 3. Receiver operating curve for ^{18}F-fluorodeoxyglucose positron emission tomography standardized uptake value (SUV). This **curve** was constructed from the SUVs of pheochromocytomas and normal adrenals in patients with nonmetastatic pheochromocytomas and paragangliomas.

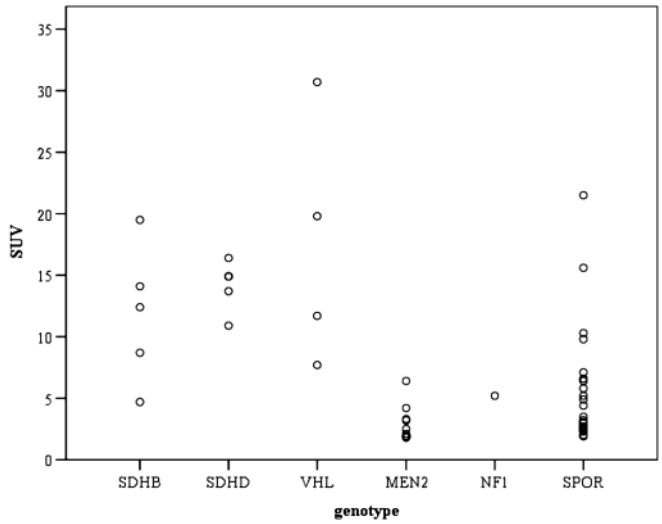

Figure 4. ^{18}F-fluorodeoxyglucose positron emission tomography standardized uptake value (SUV) in nonmetastatic pheochromocytoma and paraganglioma across genotypes. MEN2 = multiple endocrine neoplasia type 2, MN = plasma metaneprine, NF1 = neurofibromatosis type 1, NMN = plasma normetanephrine, ns = nonsignificant, SDHB/C/D/x= succinate dehydrogenase subunit B/C/D/x, SPOR = sporadic, SUVmax = maximum SUV, VHL = von Hippel–Lindau syndrome.

the disease. However, ^{123}I-MIBG remains important to establish whether patients with metastatic PPGL qualify for ^{131}I-MIBG treatment. ^{18}F-FDG PET is probably less useful for the follow-up of MEN2 and NF1 patients. ^{18}F-FDG PET also appears to be useful in the localization of HNPGL, but its role among other imaging modalities such as MRI, [^{18}F]-DOPA PET, and somatostatin receptor–based imaging remains to be determined.

One limitation of this study is that a relatively low number of hereditary nonmetastatic PPGLs were available for comparison of genotype-specific imaging results. Further studies with a larger sample size are needed to assess the full impact of the genotypes on ^{18}F-FDG uptake by PPGL and to establish the role of functional imaging in the diagnosis of underlying hereditary disorders. Also, the usefulness of ^{18}F-FDG PET for the localization of HNPGL warrants further evaluation with a larger sample size.

In conclusion, ^{18}F-FDG PET/CT scanning is suitable for routine functional imaging of PPGLs. Compared with ^{123}I-MIBG SPECT, ^{18}F-FDG PET allows better detection of metastases, provides a high specificity, and enables functional characterization of PPGL. The observations of a high ^{18}F-FDG uptake in *SDH*- and *VHL*-related tumors vs low uptake in MEN2-related tumors illustrate that functional imaging can provide important clues for a hereditary syndrome underlying PPGL.

References

1. Lenders JW, Eisenhofer G, Mannelli M, Pacak K. Phaeochromocytoma. *Lancet.* 2005;366(9486):665–675.
2. Neumann HP, Bausch B, McWhinney SR, et al. Germ-line mutations in nonsyndromic pheochromocytoma. *N Engl J Med.* 2002;346(19):1459–1466.
3. Neumann HP, Pawlu C, Peczkowska M, et al. Distinct clinical features of paraganglioma syndromes associated with SDHB and SDHD gene mutations. *JAMA.* 2004;292(8):943–951.
4. Timmers HJ, Kozupa A, Eisenhofer G, et al. Clinical presentations, biochemical phenotypes, and genotype-phenotype correlations in patients with SDHB-associated pheochromocytomas and paragangliomas. *J Clin Endocrinol Metab.* 2007;92(3):779–786.
5. Lenders JW, Pacak K, Walther MM, et al. Biochemical diagnosis of pheochromocytoma: which test is best? *JAMA.* 2002;287(11):1427–1434.
6. Hoegerle S, Nitzsche E, Altehoefer C, et al. Pheochromocytomas: detection with 18F DOPA whole body PET—initial results. *Radiology.* 2002;222(2):507–512.
7. Pacak K, Eisenhofer G, Carrasquillo JA, Chen CC, Li ST, Goldstein DS. 6-[18F]fluorodopamine positron emission tomographic (PET) scanning for diagnostic localization of pheochromocytoma. *Hypertension.* 2001;38(1):6–8.
8. Timmers HJ, Chen CC, Carrasquillo JA, et al. Comparison of 18F-fluoro-L-DOPA, 18F-fluoro-deoxyglucose, and 18F-fluorodopamine PET and 123I-MIBG scintigraphy in the localization of pheochromocytoma and paraganglioma. *J Clin Endocrinol Metab.* 2009;94(12):4757–4767.
9. Belhocine T, Spaepen K, Dusart M, et al. 18FDG PET in oncology: the best and the worst (Review). *Int J Oncol.* 2006;28(5):1249–1261.
10. Pauwels EK, Sturm EJ, Bombardieri E, Cleton FJ, Stokkel MP. Positron-emission tomography with [18F]fluorodeoxyglucose. Part I. Biochemical uptake mechanism and its implication for clinical studies. *J Cancer Res Clin Oncol.* 2000;126(10):549–559.
11. Timmers HJ, Kozupa A, Chen CC, et al. Superiority of fluorodeoxyglucose positron emission tomography to other functional imaging techniques in the evaluation of metastatic SDHB-associated pheochromocytoma and paraganglioma. *J Clin Oncol.* 2007;25(16):2262–2269.
12. Taieb D, Sebag F, Barlier A, et al. 18F-FDG avidity of pheochromocytomas and paragangliomas: a new molecular imaging signature? *J Nucl Med.* 2009;50(5):711–717.
13. Favier J, Briere JJ, Burnichon N, et al. The Warburg effect is genetically determined in inherited pheochromocytomas. *PLoS One.* 2009;4(9):e7094.
14. Burnichon N, Briere JJ, Libe R, et al. SDHA is a tumor suppressor gene causing paraganglioma. *Hum Mol Genet.* 2010;19(15):3011–3020.
15. Bayley JP, Kunst HP, Cascon A, et al. SDHAF2 mutations in familial and sporadic paraganglioma and phaeochromocytoma. *Lancet Oncol.* 2010;11(4):366–372.
16. Qin Y, Yao L, King EE, et al. Germline mutations in TMEM127 confer susceptibility to pheochromocytoma. *Nat Genet.* 2010;42(3):229–233.
17. Timmers HJ, Hadi M, Carrasquillo JA, et al. The effects of carbidopa on uptake of 6-18F-Fluoro-L-DOPA in PET of pheochromocytoma and extraadrenal abdominal paraganglioma. *J Nucl Med.* 2007;48(10):1599–1606.
18. King KS, Chen CC, Alexopoulos DK, et al. Functional imaging of SDHx-related head and neck paragangliomas: comparison of 18F-fluorodihydroxyphenylalanine, 18F-fluorodopamine, 18F-fluoro-2-deoxy-D-glucose PET, 123I-metaiodobenzylguanidine scintigraphy, and 111In-pentetreotide scintigraphy. *J Clin Endocrinol Metab.* 2011;96(9):2779–2785.
19. Miller R. *Beyond ANOVA, Basics of Applied Statistics.* New York, NY: John Wiley & Sons; 1986.
20. Bagheri B, Maurer AH, Cone L, Doss M, Adler L. Characterization of the normal adrenal gland with 18F-FDG PET/CT. *J Nucl Med.* 2004;45(8):1340–1343.
21. Eisenhofer G, Pacak K, Huynh TT, et al. Catecholamine metabolomic and secretory phenotypes in phaeochromocytoma. *Endocr Relat Cancer.* 2011;18(1):97–111.
22. Kaji P, Carrasquillo JA, Linehan WM, et al. The role of 6-[18F]fluorodopamine positron emission tomography in the localization of adrenal pheochromocytoma associated with von Hippel-Lindau syndrome. *Eur J Endocrinol.* 2007;156(4):483–487.
23. Gimenez-Roqueplo AP, Favier J, Rustin P, et al. Functional consequences of a SDHB gene mutation in an apparently sporadic pheochromocytoma. *J Clin Endocrinol Metab.* 2002;87(10):4771–4774.
24. Kaelin WG. Von Hippel-Lindau disease. *Annu Rev Pathol.* 2007;2:145–173.
25. Warburg O. On the origin of cancer cells. *Science.* 1956;123(3191):309–314.

26. Dahia PL, Ross KN, Wright ME, et al. A HIF1alpha regulatory loop links hypoxia and mitochondrial signals in pheochromocytomas. *PLoS Genet*. 2005;1(1):72–80.
27. Mann GN, Link JM, Pham P, et al. [11C]metahydroxyephedrine and [18F]fluorodeoxyglucose positron emission tomography improve clinical decision making in suspected pheochromocytoma. *Ann Surg Oncol*. 2006;13(2):187–197.
28. Shulkin BL, Thompson NW, Shapiro B, Francis IR, Sisson JC. Pheochromocytomas: imaging with 2-[fluorine-18]fluoro-2-deoxy-D-glucose PET. *Radiology*. 1999;212(1):35–41.
29. Timmers HJ, Eisenhofer G, Carrasquillo JA, et al. Use of 6-[18F]-fluorodopamine positron emission tomography (PET) as first-line investigation for the diagnosis and localization of non-metastatic and metastatic phaeochromocytoma (PHEO). *Clin Endocrinol (Oxf)*. 2009;71(1):11–17.
30. Fiebrich HB, Brouwers AH, Kerstens MN, et al. 6-[F-18]Fluoro-L-dihydroxyphenylalanine positron emission tomography is superior to conventional imaging with (123)I-metaiodobenzylguanidine scintigraphy, computer tomography, and magnetic resonance imaging in localizing tumors causing catecholamine excess. *J Clin Endocrinol Metab*. 2009;94(10):3922–3930.
31. Gimenez-Roqueplo AP, Lehnert H, Mannelli M, et al. Phaeochromocytoma, new genes and screening strategies. *Clin Endocrinol (Oxf)*. 2006;65(6):699–705.

Funding

This research was supported by the Intramural Research Program of the Eunice Kennedy Shriver National Institute of Child Health and Human Development at the National Institutes of Health (NICHD/NIH) and Pheo Para Alliance. The work leading to these results has received funding from the European Union Seventh Framework Programme (FP7/2007-2013) under grant agreement no. 259735.

Notes

The sponsors had no role in the design of the study, the collection, analysis, or interpretation of the data, the writing of the article, and the decision to submit the article for publication.

Affiliations of authors: Department of Endocrinology and Department of Laboratory Medicine, Radboud University Nijmegen Medical Centre, Nijmegen, the Netherlands (HJLMT, JUR); Program in Reproductive and Adult Endocrinology, Eunice Kennedy Shriver National Institutes of Child Health and Human Development (HJLMT, KSK, KTA, KP); Department of Nuclear Medicine (CCC, JAC, MW), Department of Radiology and Imaging Sciences (CCC, JAC, MW, AL), Warren G. Magnuson Clinical Center; Biostatistics Services (RAW), National Institutes of Health, Bethesda, MD; Nuclear Medicine Section, Department of Radiology, Memorial Sloan Kettering Cancer Center, New York, NY (JAC); Institute of Clinical Chemistry and Laboratory Medicine, Department of Medicine, Department of Clinical Chemistry, and Division Of Clinical Neurochemistry, University of Dresden, Dresden, Germany (GE).